JOURNAL OF THE KOREAN ASTRONOMICAL SOCIETY
38: 223 ~ 226, 2005

21cm RADIO CONTINUUM EMISSION SURVEY OF THE LARGE MAGELLANIC CLOUD

SUNGEUN KIM
Department of Astronomy and Space Sciences, Sejong University, Seoul, 143-747, Korea
E-mail: skim@arcsec.sejong.ac.kr
(Received February 1, 2005; Accepted March 15, 2005)

ABSTRACT

We present the results of a 21cm radio continuum aperture synthesis mosaic of the Large Magellanic Cloud (LMC), made by combining data from 1344 separate pointing centers using the Australia Telescope Compact Array (ATCA) and the 64-m Parkes single-dish telescope. The resolution of the mosaicked images is 55" (10 pc, using a distance to the LMC) and a region $10° \times 12°$ is surveyed.

Key words : radio continuum — aperture synthesis — galaxies: individual (LMC) — atomic

I. INTRODUCTION

The Large Magellanic Cloud (LMC) presents us with a uniquely favorable case for studying the connection between the processes of star formation and the structure and dynamics of the interstellar medium (ISM) in galaxies. It is the nearest disk galaxy to our own and seen at a small inclination so that confusion along the line of sight is negligible. Its internal reddening is low as typically E_{B-V}=0.13 (Massey et al. 1995) as and it is near enough that its stellar populations can be studied in detail. As such, it fills an important role in helping us bridge the gap between our understanding of the small-scale structure of the ISM gleaned from studies of our Galaxy and the global processes seen in more distant galaxies. In addition, the LMC is known to be interacting with both the halo of our Galaxy and with its smaller companion, the Small Magellanic Cloud (SMC).

HI aperture synthesis mosaicked map of the LMC taken by the Australia Telescope Compact Array (ATCA) and the Parkes 64-m radio single-dish telescope (Kim et al. 2003) proves the complex system of filamentary structures, combined with numerous HI holes and shells (Kim et al. 1999). The HI supergiant shells are prominent in the ATCA+Parkes map of the LMC. Many HI shells are found in regions of very active star formation in the LMC and they obviously form a very complex structure of the ISM.

The canonical model for hole and shell formation is the evacuation of the cool interstellar medium (ISM) by the combined kinetic and radiation pressure stellar winds from massive stars and supernovae in the ionized hydrogen medium and star-forming regions over a period of time (Weaver et al. 1977; McCray & Kafatos 1987). The largest shells, sometimes called supershells or supergiant shells, require input energies over 10^{54} ergs (Ryder et al. 1995; van der Hulst & Sancisi 1988) to account for their formation. This is the equivalent of over 10^3 supernovae (SNe). In disk galaxies, much of the swept-up material is able to vent into the halo (Thilker et al. 1998) and therefore contribute to the "galactic chimney" (Norman & Ikeuchi 1989; Heiles 1979) and play an important role in the chemical and dynamical evolution of the multi-phase ISM. However, in general, there appears to be a weak correlation between the HI shells and the OB stars (Massey et al. 1995) as well as the ionized gas traced out by the HII regions and HII shells in the LMC. If massive star formation is the ultimate causal factor of the HI shells and supershells, this clearly shows that the life time of HI shells must be longer than the lifetime of the OB stars that input the energy required to drive the expansion of the HI shells. But this seems not to be true since the shells are, in general, younger than the mean age of the stars of the apparent OB association in the LMC.

In this paper, we present a 21cm radio continuum image of the LMC, obtained with the Australia Telescope Compact Array (ATCA) at the Australia Telescope National Facility (ATNF), in order to compare with the shells seen in the HI map of the LMC. We also discuss the properties of radio continuum emission in the LMC.

II. OBSERVING STRATEGY AND PARAMETERS

The LMC has been observed with the ATCA and the Parkes 64-m single-dish telescope. The ATCA is an east-west radio interferometer, situated near Narrabri in Australia. The telescope is at latitude – 30° 18′. The ATCA consists of five antennaes located along a 3 km rail track, and a sixth antennae 3 km further to the west. For the LMC observations, four 750 m configurations (five antennaes spread over ~ 750 m) of the ATCA has been used in 1994 October 26 – November 9 (750D), 1995 February 23 – March 11 (750A), 1995 June 2 – 7 and 1995 October 15 – 31 (750B), and 1996

Proceedings of *the 6th East Asian Meeting of Astronomy*, held at Seoul National University, Korea, from October 18-22, 2004.

January 27 – February 8 (750C). The combined configuration has 40 independent baselines ranging from 30 to 750 m, with a baseline increment of 15.3 m. This results in an angular resolution of 55" for the data presented here. A region of 10° × 12° covering the LMC centered on $\alpha = 05^{\rm h}20^{\rm m}$, $\delta = -68°44'$ (J2000) was surveyed into 12 regions, each one containing 112 pointing centers. The array was cycled around 112 adjacent pointing centers in a raster pattern and each pointing center was observed for 15.0 s (which includes 3.9s for the antennae drive). The pointing grid pattern follows a hexagonal grid which is guided by Nyquist's sampling theorem. The angular separation of pointings, θ_{hex}, for such a grid, is

$$\theta_{hex} = \frac{2}{\sqrt{3}} \frac{\lambda}{2D}, \quad (1)$$

(λ being the wavelength, and D being the dish diameter). This gives a 19 arcmin grid spacing at 21cm in Fig. 1. The pointing centers were placed on a hexagonal grid of side 19 arcmin. The continuum and HI line observations were made simultaneously for a total integration time of 900 min for each position within the LMC. The continuum images were extracted from a bandwidth of 156 kHz centered at 1420.2 MHz and a bandwidth of 234 kHz centered at 1418.2 MHz.

To provide the complete map at low spatial resolution to complement the ATCA data, observations were taken with the inner 7 beams of the Parkes Multibeam receiver on 1998 December 13 to 17. The receiver was scanned across the LMC in orthogonal east-west and north-south great circles and the receiver was continuously rotated such that the rotation angle was always 19°.1 to the scan trajectory, thus ensuring uniform spatial sampling of the sky. The area covered was 13° by 14° in RA and Dec., respectively and centered on 15^h20^m, -68°44′ (J2000). In a single scan, the spacing between adjacent tracks is 9′.5, which is smaller than the mean FWHP beam width of 14′.1, but greater than the Nyquist interval ($\lambda/2D$) of 5.′7. Therefore, six scans are interleaved in each of the principal scan directions, resulting in a final track spacing of 1.′6. In total, 12×6 RA scans and 11×6 Dec. scans were made. Seven scans were dropped or edited out due to drive problems, leaving a total of 131 scans consisting of a total of 29 hours of on-source integration on each of 7 beams. The average integration time per beam area is 360 seconds for both polarizations.

The interferometer and single-dish images are added together before deconvolution, and then deconvolution performed with a modified point-spread function (Schwarz & Walker 1991). As the Parkes and ATCA images give accurate representations of the LMC at short spacings and mid to long spacings respectively, a composite image can be formed by filtering out the short spacing data from the ATCA data (Fig. 2) and then adding the Parkes image. This process is most easily visualized in the Fourier domain and the Fourier transform of the Parkes images were added to the final images with no weighting. The deconvolved ATCA data was also Fourier-transformed, but by down-weighting the lower spatial frequencies such that the combined weight of the Parkes and ATCA data was the same as the response to a 55" Gaussian. The MIRIAD task IMMERGE was used.

Before combining, the Parkes image was interpolated onto the same coordinate grid as the ATCA mosaicked image. Also the residual primary beam attenuation remaining in the ATCA image was applied to the Parkes image (the mosaicing process we have used does not perform full primary beam correction when this would result in excessive noise amplification). In order to perform the combination of the Parkes and ATCA observations, we need to ensure that the flux calibration between the two data types are consistent. Ideally we would like to find the ratio of the flux density of an unresolved point source in the field. We have estimated this calibration factor by examining data in the Fourier plane between 21 and 31 meters - data in this annulus is well measured by the Parkes and mosaicked ATCA observations. We tapered the ATCA data to the same resolution as the Parkes data and minimized the L_1 difference between the interferometer and single-dish Fourier components and the real and imaginary parts of the data where treated as distinct measurements in the fitting. Of-course this requires a good estimate of the resolution of the Parkes image.

III. 21cm RADIO CONTINUUM MAP OF THE LMC

In Fig. 3, we display the 21cm radio continuum contour map from the combined ATCA map with the Parkes single dish map and compare with ATCA+Parkes combined map. The individual background sources are clearly seen in the continuum map. Both HI ATCA map and HI ATCA+Parkes combined map has shown that the HI distribution is uniform and no bar corresponding to the optical bar. Neither 21cm radio continuum map has corresponding bar feature. However, the diffuse radio continuum emission traces well the Hα emission of the LMC (Kim et al. 1999). Many diffuse continuum emission features are associated with the expanding shells. However, most of them are likely to originate from the HI cloudlets along the rim of shells rather than inner parts of shells. These HI cloudlets may be formed by acceleration as a result of the motion induced by the expanding giant shell surrounding HI hole. Although radio continuum emission might have contributed to the external heating of the molecular material and have transfered the molecular hydrogen to the atomic hydrogen.

IV. DISCUSSION

The structure of the radio continuum emission in the LMC shows a complex distribution of hundreds of background sources, HII regions, supernovae remnants, and

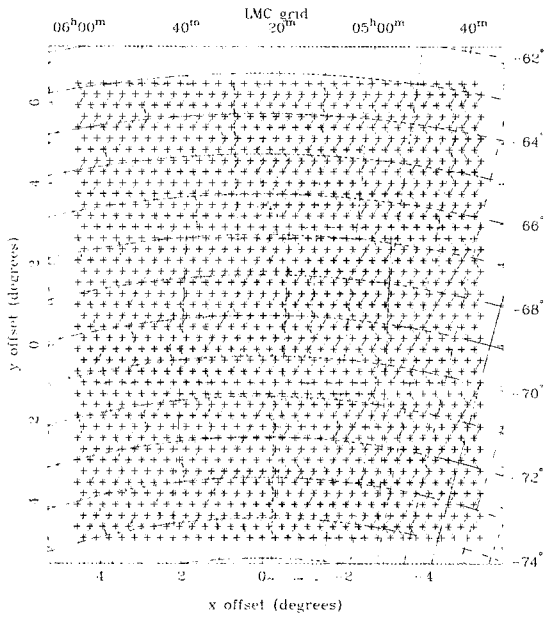

Fig. 1.— Pointing centers of ATCA mosaic survey: the LMC was divided into 12 regions and surveyed. Each region contained 112 pointing centers, 14 in Dec (shown joined) and 8 in RA. The total number of pointing centers was 1344.

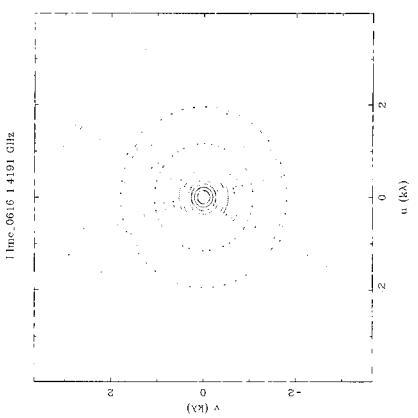

Fig. 2.— The Compact Array uv-coverage of LMC pointing 616 at $05^h04^m15.5^s$, -66°44′26" (J2000). This is the middle pointing of the 112 pointings in the 6th observing field (see Fig. 1), and is quite typical. Mosaicing improves the uv-coverage further.

diffuse background emission. Compared to the large scale distribution, the small-scale structures seen in the ATCA map (e.g. Fig. 4) still dominate the structure of the radio continuum emission in the LMC revealed by the ATCA+Parkes combined map. To compare with the structure of the HI map of the LMC, here we revisit properties of the HI emission features.

The HI emission from the LMC has been redefined as HI clouds or clumps (Kim et al. 2003). Kim et al. (2003) have identified and catalogued HI clouds in the LMC by defining a cloud to be an object composed of all pixels in right ascension, declination, and velocity that are simply connected and that lie above the threshold brightness temperature. HI clouds and clumps were found using the automatic clump identification code by Lee et al. (1997). Final selection of HI clouds has been made with high-temperature thresholds in order to reduce the blending of emission from unrelated clouds. The derived sizes of clouds were distributed in a wide range of scales 20 – 400 pc. Peak of their size distribution of HI clouds or clumps resides in 20 – 30 pc. However, the effective synthesis beam size 55" limits the size distribution of the smallest HI clouds. The data are consistent with a power-law distribution with slope of between $s = -0.9 \pm 0.2$ and $s = -1.1 \pm 0.2$. Compared to the slope found from the size spectrum of CO clouds in the inner Galaxy, -2.43±0.05 (Solomon et al. 1987); Ophiuchus, -2.20±0.06; Rosette, -2.26±0.08; Maddalena-Thaddeus, -2.46 ± 0.20; M17, -2.09 ± 0.18 (Falgarone et al. 1995), the power-law distribution of the size spectrum of HI clouds is flatter than the typical size spectrum of CO clouds in the Milky Way. In Fig. 4 the measured perimeter P and measured enclosed area A of each HI cloud in a log-log plot gives a set of points lying along with a slope of $D/2 = 0.73 \pm 0.1$. The relation between area and perimeter of each identified HI cloud, P is proportional to $A^{D/2}$, can determine the fractal dimension $D = 1.47 \pm 0.2$ of a cloud boundary (Vogelaar & Wakker 1994; Williams, Blitz, & McKee 2000). The measured fractal dimension of HI clouds in the LMC is a similar dimension, $D \pm 1.4$, found in many studies of the molecular ISM (Falgarone et al. 1991; Williams, Blitz, & McKee 2000). For clouds identified with different thresholds of the brightness temperature, the fractal dimension D found from the relation between area and perimeter is invariant as shown in Fig. 5 (Kim et al. 2003). A fractal analysis of diffuse radio continuum is being underway and the result of the analysis will be compared to that of HI clouds in a separate paper.

ACKNOWLEDGEMENTS

We are grateful to LMC ATCA survey project team members. This work was supported by Korea Science & Engineering Foundation (KOSEF) under a cooperative agreement with the Astrophysical Research Center of the Structure and Evolution of the Cosmos (ARCSEC).

REFERENCES

Falgarone, E., Phillips, T.G., & Walker, C. K., 1991, ApJ, 378, 186

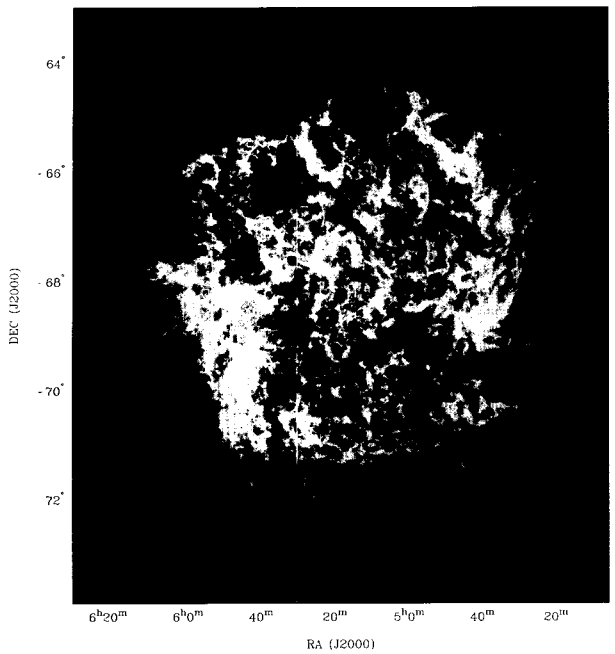

Fig. 3.— 21cm radio continuum emission to the same scale as HI emission. Contour map represents 21cm radio continuum emission.

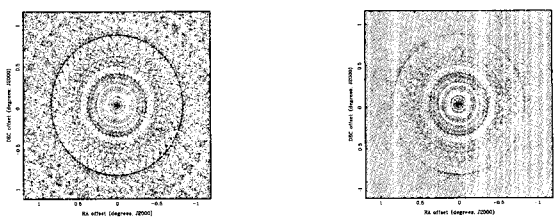

Fig. 4.— Point responses from ATCA mosaic observations. A synthesized beam from the pointing center is shown on the left and the PSF at the same position of the mosaic is shown on the right. Both displays are saturated at the level ± 0.1.

Heiles, C., 1979, ApJ, 229, 533

Kim, S., Staveley-Smith, L., Dopita, M. A., Freeman, K. C., Sault, R. J., Kesteven, M. J., & McConnell, D., 1998, ApJ, 503, 674

Kim, S., Dopita, M.A., Staveley-Smith, L., & Bessell, M., 1999, AJ, 118, 2797

Kim, S., Staveley-Smith, L., Dopita, M. A., Sault, R. J., Freeman, K. C., Lee, Y., Chu, Y.-H., 2003, ApJS, 148, 473

Lee, Y., Jung, J., & Kim, H. G., 1997, PKAS, 12, 111

McCray, R., & Kafatos, M., 1987, ApJ, 317, 190

Massey, P., Lang, C. C., Degioia-Eastwood, K., & Garmany, C. D., 1995, ApJ, 438, 188

Norman, C. A., & Ikeuchi, S., 1989, ApJ, 345, 372

Ryder, S. D., Staveley-Smith, L., Malin, D., & Walsh, W., 1995, AJ, 109, 1592

Solomon, P. M., Rivolo, A. R., Barrett, J., & Yahil, A., 1987, ApJ, 319, 730

Thilker, D. A., Braun, R., & Walterbos, R. M. 1998, A&A, 332, 429

van der Hulst, J. M., & Sancisi, L., 1988, AJ, 95, 1394

Vogelaar, M. G. R., & Wakker, B. P., 1994, A&A, 291, 557

Weaver, R., McCray, R., Castor, J., Shapiro, P., & Moore, R., 1977, ApJ, 218, 377

Williams, J. P., Blitz, L., & McKee, C. F., 2000, in *Protostars and Planets IV*, eds. Mannings, V., Boss, A.P., & Russell, S. S. (Tucson: University of Arizona Press), 97

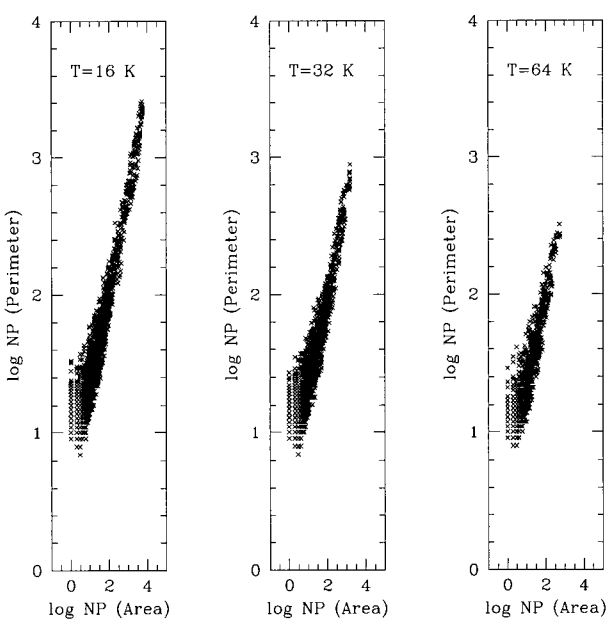

Fig. 5.— A log-log plot of the measured perimeter versus the measured area in units of pixels of HI clouds for three thresholds of the brightness temperature, T_B = 16K, 32K, 64K.